RESEARCH ARTICLE
doi: 10.2306/scienceasia1513-1874.2026.050

ScienceAsia 52 (3): 2026: ID 2026050: **1–9**

Independent optimization of pitch coating and second-level prelithiation for enhancing the lithium storage performance of anthracite coal-based graphite anodes

Canliang Ma[a,*], Ruyi Li[a], Jiao Che[a], Yun Zhao[a], Ruibin Ma[a], Ning-jing Song[b], Xiaoming Li[c]

[a] Key Laboratory of High-Performance Energy Storage Materials and Systems of Shanxi Province, Institute of Molecular Science, Shanxi University, Taiyuan 030006 China
[b] Department of Materials Science and Engineering, Jinzhong University, Jinzhong 030619 China
[c] CAS Key Laboratory of Carbon Materials, Institute of Coal Chemistry, Chinese Academy of Sciences, Taiyuan 030001 China

*Corresponding author, e-mail: macanliang@sxu.edu.cn

Received 9 Dec 2025, Accepted 13 May 2026
Available online 29 May 2026

ABSTRACT: To enhance the performance of anthracite-coal-based graphite anodes for lithium-ion batteries, this study independently optimized pitch coating and second-level contact prelithiation strategies. Systematic parameter screening led to the construction of a graphitic core–amorphous carbon shell composite anthracite-based synthetic graphite (SBG@P230-10%-C1000) using P230 pitch (10 wt%) carbonized at 1000 °C. Characterization confirmed an expanded interlayer spacing (0.3418 nm) and a 49.6% reduction in specific surface area (1.866 m^2/g), promoting Li^+ diffusion and suppressing excessive Solid Electrolyte Interphase (SEI) formation. Electrochemically, the coated anode achieved an Initial Coulombic Efficiency (ICE) of 81.82% at 50 mA/g and a high-rate capacity of 104.5 mAh/g at 3200 mA/g, which is 2.56 times that of pristine anthracite-based synthetic graphite (SBG). A 20 s direct contact prelithiation treatment further increased the ICE to 97.32% and maintained a capacity of 389.55 mAh/g after 100 cycles at 100 mA/g. The individually optimized strategies for coating and prelithiation highlight a promising combined approach to overcome the low ICE and poor rate capability of coal-based graphite, supporting its potential application in high-performance silicon-carbon anode systems.

KEYWORDS: lithium-ion batteries, anthracite coal-based graphite anode, pitch coating, prelithiation, rate capability, Coulombic efficiency

INTRODUCTION

Graphite remains the dominant anode material for lithium-ion batteries due to its excellent comprehensive performance [1, 2]. Even in next-generation silicon-carbon composites, graphite constitutes 50–90% of the system to ensure structural integrity and conductivity [3, 4]. The demand for higher energy density and fast-charging capabilities makes developing low-cost graphite anodes with high initial Coulombic efficiency (ICE) and superior rate performance a critical priority [5, 6].

Currently, the graphite anode market relies heavily on petroleum-based needle coke, which suffers from price volatility and low graphitization yield (< 85%) [7]. Anthracite coal (carbon content > 90%), abundant in regions like Shanxi, China, offers a promising alternative. Its carbon-rich nature shortens the graphitization process, yielding over 80% graphitized product [8], and its microcrystalline structure is suitable for high-performance anodes [1, 9, 10]. Our previously developed SBG reduced raw material costs by 40%. However, its ICE (80.52%) and rate capability (40.8 mAh/g at 3200 mA/g) require further improvement.

Amorphous carbon coating is an effective strategy for enhancing graphite anodes [11, 12]. Its isotropic structure facilitates rapid Li^+ diffusion, improving rate performance [13], and its minimal volume change enhances cycling stability [14]. For instance, asphalt coating repairs defects in recycled graphite [15], and chemical vapor deposition of carbon layers improves the kinetics [16]. Concurrently, prelithiation compensates for the irreversible lithium consumption during initial SEI formation, which is the primary cause of low ICE [17]. Among various methods [18–20], electrochemical prelithiation is notable for its operational simplicity and precise control [20, 21], although most techniques require several minutes, posing efficiency and safety challenges [22]. Research on second-level prelithiation for coal-based graphite is particularly scarce.

While pitch coating and prelithiation have each demonstrated considerable potential, the independent optimization of these two strategies for SBG—particularly the parameters for pitch coating and the timing of second-level contact prelithiation (< 60 s)—remains insufficiently explored. This work systematically and separately refines both approaches to address the performance limitations of SBG. The objectives are: (1) to identify the optimal pitch-coating parameters—including softening point, coating amount, and carbonization temperature—for constructing a graphitic core–amorphous carbon shell structure; (2) to de-

termine the ideal duration for second-level contact prelithiation (10–40 s) to maximize the ICE; and (3) to separately analyze the individual contribution of each independently optimized strategy to the electrochemical performance, thereby providing a clear mechanistic basis for enhancing the ICE and rate capability of coal-based graphite anodes, respectively.

MATERIALS AND METHODS

Material preparation

Anthracite coal-based graphite (SBG) was used as the coating substrate. Composites were prepared via a solution coating–heat treatment method. The brief procedure is as follows: precise amounts of SBG and pitch (P-series) with specific softening points were dissolved in 50 ml of N-methyl-2-pyrrolidone (NMP) solvent. The mixture was heated and stirred using a magnetic stirrer until a complete coating was achieved. The resulting precursor was dried in an oven at 80 °C for 12 h. After grinding, the precursor was placed in a tube furnace and subjected to heat treatment (carbonization temperature: 800–1200 °C, duration: 1 h) under an argon atmosphere, yielding the final SBG@PC composite.

Experimental parameter optimization design

The effects of pitch coating parameters were systematically investigated through single-factor experiments, with the specific experimental design as follows: 1) Effect of pitch softening point: Fixed parameters: 1.8 g graphite, 0.2 g pitch (10 wt%), 50 ml NMP, and a carbonization temperature of 1000 °C. Variable: pitch softening point (140, 230, and 270 °C); 2) Effect of carbonization temperature: Fixed parameters: a pitch softening point of P230, a coating amount of 10 wt%. Variable: carbonization temperature (800, 1000, and 1200 °C); 3) Effect of coating amount: Fixed parameters: a pitch softening point of P230, a carbonization temperature of 1000 °C, and 50 ml NMP. Variable: pitch coating amount (5, 10, and 15 wt%). The resulting products were designated as SBG@Px-y%-Cz (where x represents the softening points of 140, 230, and 270; y represents the pitch amounts of 5%, 10%, and 15%; and z represents the carbonization temperatures of 800, 1000, and 1200 °C).

Characterization and testing methods

The phase composition and crystal structure of the samples were analyzed by X-ray diffraction (XRD, D8 Advance, Bruker, Germany) and Raman spectroscopy (Raman, LabRAM HR Evolution, Horiba, Japan). The morphology and microstructure of the samples were analyzed by scanning electron microscopy (SEM, JSM-7001F, JEOL, Japan) and transmission electron microscopy (TEM, JEM-2800, JEOL). The specific surface area and pore size distribution of the samples were measured by a specific surface area analyzer (BET, ASAP2460, Micromeritics, Norcross, GA, USA).

Electrochemical performance was evaluated using CR2016 coin cells. The working electrode was prepared by mixing the active material, carboxymethyl cellulose (CMC), and acetylene black in a mass ratio of 8:1:1. An appropriate amount of deionized water was added, and the mixture was ground into a slurry, which was then uniformly coated onto copper foil using a coater. The coated foil was dried in a vacuum oven at 120 °C for 12 h. After drying, it was cut into 12-mm diameter discs using a punching machine. The active material mass loading on the electrode was controlled between 1.4 and 1.6 mg/cm^2. Coin-type half-cells (CR2016) were assembled in an argon-filled glovebox (H_2O, $O_2 < 1$ ppm) using the prepared electrode as the working electrode, a lithium metal sheet as the reference/counter electrode, a polypropylene membrane as the separator, and 1 M $LiPF_6$ in EC/DMC (1:1 v/v) as the electrolyte.

Prelithiation was performed by dropping 20 µl of electrolyte onto the electrode surface to ensure sufficient interfacial reaction, placing a fresh lithium foil (12 mm in diameter, 0.45 mm in thickness, $\geqslant$ 99.9% purity) on top, and applying a constant pressure of approximately 0.173 MPa (using a 200 g weight) to ensure full contact, with the contact time controlled (10 s, 20 s, and 40 s). After prelithiation, the cells were assembled following the standard procedure.

RESULTS AND DISCUSSION

Systematic optimization of pitch coating parameters (softening point, carbonization temperature, and coating amount) was conducted to enhance the performance of SBG. The morphological evolution under different conditions is revealed by SEM analysis. Compared to the pristine SBG with exposed edges and corners (Fig. 1a), significant morphological changes occurred after coating. P140 pitch (Fig. 1b) resulted in a discontinuous and non-uniform layer. In contrast, P230 pitch (Fig. 1c) formed a uniform, continuous, and wrinkled carbon layer, achieving complete encapsulation of the graphite core. However, P270 pitch (Fig. 1d) caused obvious particle agglomeration and a cracked coating. These results indicate that P230, with its appropriate viscosity, achieves an optimal balance for forming a dense and continuous coating. The carbonization temperature critically determines the coating's structure. The sample treated at 800 °C (Fig. 1e) showed a rough and porous surface, indicating insufficient carbonization.

The sample carbonized at 1000 °C (Fig. 1c) exhibited an ideal, dense, and uniform coating, successfully constructing a graphitic core-amorphous carbon shell structure. Conversely, the surface of the sample treated at 1200 °C (Fig. 1f) became overly smooth, showing signs of densification and shrinkage, which could lead to microcracks due to excessive graphitization. A tem-

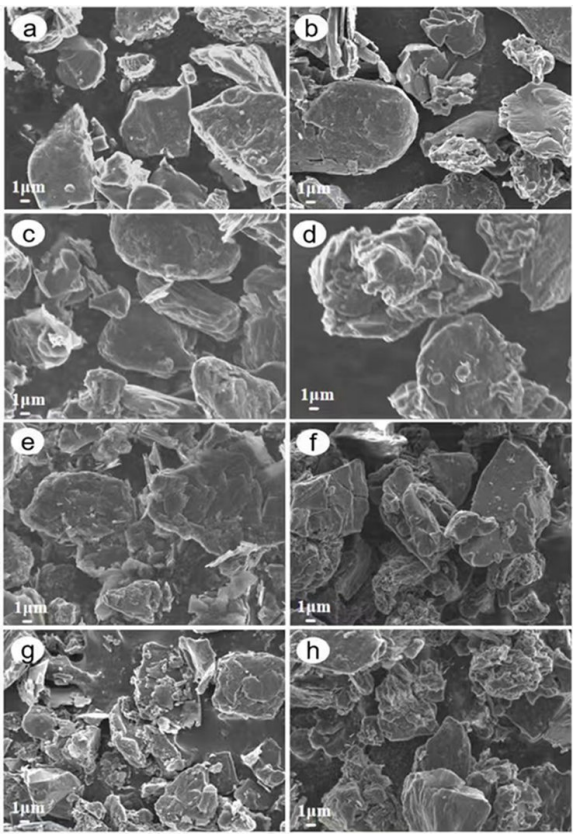

Fig. 1 SEM images of (a) SBG, (b) SBG@P140-10%-C1000, (c) SBG@P230-10%-C1000, (d) SBG@P270-10%-C1000, (e) SBG@P230-10%-C800, (f) SBG@P230-10%-C1200, (g) SBG@P230-5%-C1000, and (h) SBG@P230-15%-C1000.

perature of 1000 °C provides the optimal trade-off. The coating amount directly governed the coverage and thickness. A 5% coating amount (Fig. 1g) led to incomplete coverage, with graphite edges still exposed. A 10% coating amount (Fig. 1c) achieved a uniform and continuous layer for ideal core-shell structure construction. In contrast, a 15% coating amount (Fig. 1h) resulted in an overly thick coating, particle agglomeration, and delamination. Thus, the 10% coating amount achieves synergistic optimization between complete coverage and efficient transport.

As shown in Fig. 2 and Table 1, all samples retain the characteristic graphite diffraction peaks (e.g., (002) at ∼26.5°), confirming the pitch coating does not alter the fundamental graphite crystal structure [23, 24]. The (002) peak profile varies systematically: SBG@P140-10%-C1000 shows a broadened peak (high disorder), SBG@P230-10%-C1000 exhibits a sharp, moderately intense peak ("appropriately ordered"), while SBG@P270-10%-C1000 has high intensity with slight broadening (a tendency for excessive graphitization). Increasing temperature from

Table 1 Crystal structure parameters of SBG-based graphite samples.

Sample name	2θ (°)	FWHM (rad)	Lc (nm)
SBG	26.21666	0.016352	8.61
SBG@P140-10%-C1000	26.27708	0.016105	8.84
SBG@P230-10%-C1000	26.29723	0.012245	11.63
SBG@P270-10%-C1000	26.31737	0.013974	10.19
SBG@P230-10%-C800	26.05000	0.014835	9.59
SBG@P230-10%-C1200	26.40000	0.011345	12.55
SBG@P230-5%-C1000	26.41808	0.016459	8.66
SBG@P230-15%-C1000	25.79367	0.011922	11.93

Table 2 Specific surface area and pore properties of SBG and SBG@P230-10%-C1000.

Sample	Specific surface area (m^2/g)	Pore volume (cm^3/g)	Pore size (nm)
SBG	3.701	0.429	7.406
SBG@P230-10%-C1000	1.866	0.685	2.295

800 °C to 1200 °C sharpens the (002) peak, indicating enhanced graphitization. SBG@P230-10%-C1000 (1000 °C) represents an intermediate, optimally ordered state, whereas the 1200 °C sample shows excessive graphitization, potentially hindering ion diffusion [23, 25]. Increasing the coating amount from 5% to 15% decreases the (002) peak intensity, indicating a higher proportion of amorphous carbon and signal "dilution" from the thick coating layer [26].

The I_D/I_G ratio increased from 0.6 (pristine SBG) to 0.77 for SBG@P230-10%-C1000, confirming the successful introduction of a disordered amorphous carbon coating layer, rich in defects and grain boundaries [27]. This defect engineering optimizes interfacial ion transport pathways [28].

As shown in Fig. 2 and Table 2, pitch coating drastically reduced the specific surface area by nearly half, from 3.701 m^2/g (SBG) to 1.866 m^2/g (SBG@P230-10%-C1000). The Type IV isotherm with a hysteresis loop confirms mesoporosity [29]. The marked reduction in specific surface area confirms that the coating effectively covers and seals the original surface cracks and pores of the SBG, thereby suppressing excessive SEI formation. Although the total pore volume increases (Table 2)—likely due to mesopore formation within the amorphous carbon coating during carbonization—the concurrent decrease in average pore size implies limited accessibility of these pores to the electrolyte. Thus, they contribute minimally to the active surface area. This configuration, primarily featured by the amorphous carbon structure, facilitates rapid ion transport, achieving an optimal balance between high initial Coulombic efficiency and superior rate capability [28]. In summary, the combined structural analyses confirm that the optimal coating parameters (P230, 1000 °C, 10%) successfully construct a composite material with a moderately ordered

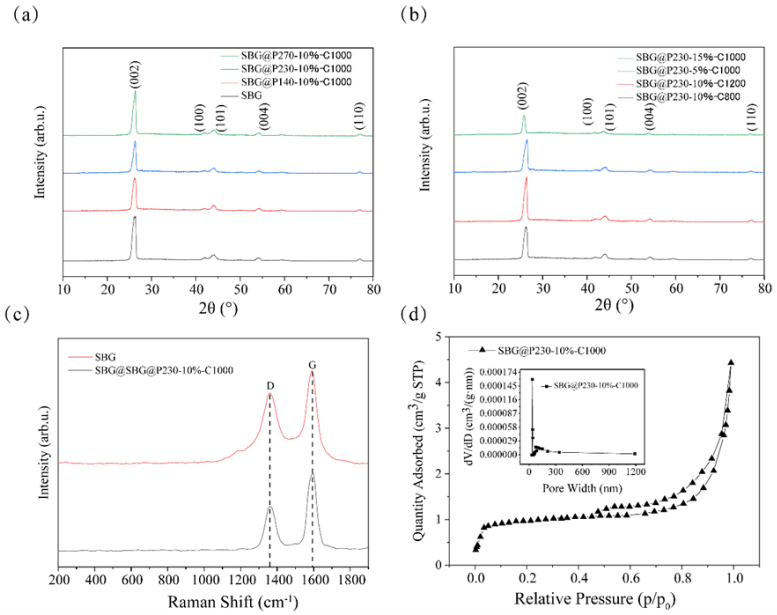

Fig. 2 XRD patterns of SBG-based graphite samples (a, b); Raman results of SBG and SBG@P230-10%-C1000 (c); nitrogen adsorption-desorption isotherm curve and pore size distribution of SBG@P230-10%-C1000 (d).

amorphous carbon shell on a graphitic core, featuring a reduced specific surface area and enhanced defect density, which collectively provide the structural foundation for the observed electrochemical improvements.

Fig. 3 presents TEM and HRTEM analyses; Fig. 3a,b provide nanoscale evidence for the performance enhancement induced by pitch coating. In stark contrast to the uncoated SBG with exposed edges and step-like defects, the optimized SBG@P230-10%-C1000 sample exhibits a uniform, continuous amorphous carbon coating (∼5–50 nm thick), successfully constructing a graphitic core-amorphous carbon shell structure (Fig. 3c–f). This coating completely encapsulates the graphite, isolating it from the electrolyte and providing the structural basis for the improved ICE by reducing active sites for side reactions. HRTEM analysis further confirmed the successful construction of the graphitic core-amorphous carbon shell structure (Fig. 3c–f). The measured interlayer spacing of the coated sample was 0.3418 nm. More importantly, the uniform amorphous carbon coating (∼5–50 nm thick) completely encapsulates the graphite core. This coating, with its isotropic structure and rich defects/grain boundaries (as indicated by the increased I_D/I_G ratio), is known to facilitate rapid Li^+ transport [30, 31]. The intimate interfacial contact and the "cloud-like" contrast indicative of structural defects within the coating layer synergistically contribute to a multifunctional balance between interface protection, enhanced ion transport, and efficient electron conduction.

Fig. 4 presents the electrochemical performance (cycling and rate capability) of SBG anodes, systematically evaluating the impact of pitch coating parameters (softening point, carbonization temperature, and coating amount). As shown in Fig. 4a,b, SBG@P230-10%-C1000 delivered superior performance, with an ICE of 81.82% and a high-rate capacity of 104.5 mAh/g at 3200 mA/g. This significantly outperformed SBG@P140-10%-C1000 (an ICE of ∼80% and a capacity of ∼79 mAh/g) and SBG@P270-10%-C1000 (an ICE of ∼75% and a capacity of ∼30 mAh/g). The optimal viscosity of P230 facilitated a continuous, dense coating for effective interface stabilization and ion transport, whereas P140 resulted in uneven coverage and P270 caused agglomeration and cracking. SBG@P230-10%-C1000 demonstrated balanced performance. In contrast, as shown in Fig. 4c,d, SBG@P230-10%-C800, with insufficient carbonization, showed a poor rate capacity (∼40 mAh/g). SBG@P230-10%-C1200, despite high crystallinity, suffered from excessive graphitization leading to hindered ion diffusion and a low-rate capacity (∼31 mAh/g), confirming 1000 °C achieves optimal "moderate graphitization". The 10% coating amount achieved the ideal balance, yielding the highest ICE and rate performance. A 5% coating led to incomplete coverage and inferior performance (an ICE of ∼80% and a capacity of ∼60 mAh/g). A 15 % coating caused kinetic hysteresis due to an overly thick layer, reducing the high-rate capacity to ∼50 mAh/g. In summary, the systematic parameter screening conclusively identifies P230 pitch, a carbonization temperature of 1000 °C, and a coating amount of 10 wt%

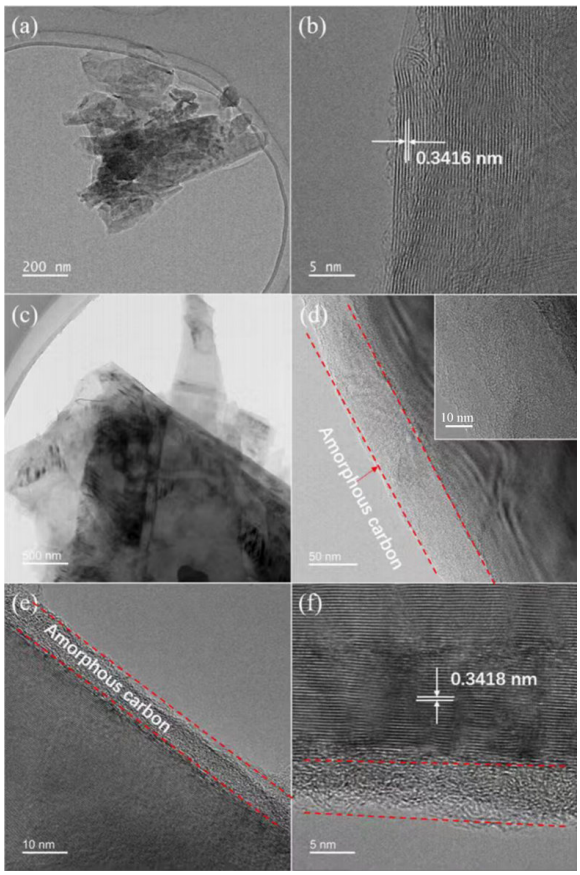

Fig. 3 TEM image (a) and HRTEM image (b) of SBG; TEM images (c, d) and HRTEM images (e, f) of SBG@P230-10%-C1000.

as the optimal combination for constructing a high-performance graphitic core-amorphous carbon shell anode, effectively enhancing both interfacial stability and ion transport kinetics [30–32].

Fig. 4e–g presents the CV and EIS analyses, providing dynamic electrochemical evidence for the performance enhancement mechanism of the pitch-coated anode. The CV curves (Fig. 4e,f) reveal a markedly weaker SEI formation peak at ∼0.6 V for SBG@P230-10%-C1000 compared to pristine SBG, confirming suppressed irreversible side reactions, which aligns with the BET-measured 49.6% reduction in specific surface area and explains the improved ICE (81.82%). Furthermore, the sharper and more symmetrical Li+ intercalation/deintercalation peaks with a reduced potential difference (ΔE_p) indicate enhanced reaction reversibility and lower polarization [33]. This kinetic improvement primarily stems from the ion-conductive amorphous carbon coating, which provides more active sites and lower-energy pathways for Li+ intercalation [34].

Electrochemical impedance spectroscopy (EIS) Nyquist plots (Fig. 4g) demonstrate that the SBG@P230-10%-C1000 electrode exhibits a smaller high-frequency semicircle, with a charge transfer resistance (R_{ct}) of 79.44 Ω, much lower than the 346.5 Ω of the pristine SBG electrode [35]. This decrease originates from the higher interfacial ionic conductivity provided by the isotropic amorphous carbon and the formation of a thinner, more stable SEI film. The lower R_{ct} directly correlates with the superior rate capability, confirming faster electrochemical reaction kinetics at the optimized interface [36].

Fig. 5 systematically evaluates the effect of contact prelithiation duration on the electrochemical performance of SBG anodes. The open-circuit voltage (OCV) decreased continuously with contact time, from 2.54 V (0 s) to 0.5 V (40 s), confirming spontaneous lithium incorporation. The optimal prelithiation time was determined to be 20 s, which dramatically increased the ICE from 80.52% to 97.32%, indicating nearly complete compensation for the initial irreversible lithium loss. A shorter duration (10 s) resulted in insufficient compensation (ICE = 92.54%), while a longer duration (40 s) led to hazardous overlithiation, as evidenced by an anomalous ICE of 102.28%. This > 100% efficiency likely stems from the oxidation of excess metallic lithium deposited on the electrode surface during prolonged contact, which contributes extra capacity during the subsequent charge process. The first-cycle charge/discharge curves visually confirm these findings. The 20 s-prelithiated electrode exhibited a closely matched charge/discharge capacity (365.20/375.28 mAh/g), demonstrating high reversibility. After 100 cycles at 100 mA/g, the 20 s sample achieved the highest capacity retention of 389.55 mAh/g, significantly outperforming the others, underscoring the dual benefits of precise lithium compensation and the formation of a stable artificial SEI layer. As shown in Fig. 5e,g, dQ/dV analysis provides mechanistic insight. The 20 s sample showed suppressed SEI formation peaks and sharper Li^+ intercalation/deintercalation peaks even at the 105th cycle, indicating excellent interfacial stability and reversibility. In contrast, the untreated and the over-lithiated (40 s) samples exhibited significant side reaction peaks or abnormal signals, respectively. In conclusion, the 20 s contact prelithiation is a highly effective strategy for overcoming the low ICE of SBG anodes. It can be seen that short-time prelithiation treatment of SBG graphite can significantly improve ICE and cycling stability performance, which is similar to the literature reports [17, 19, 21], proving that short-time second-level contact prelithiation is a simple and effective method to enhance the electrochemical performance of graphite anodes.

Fig. 6 synthesizes the independent optimization results of pitch coating and prelithiation, outlining the logical foundation for their combined use towards

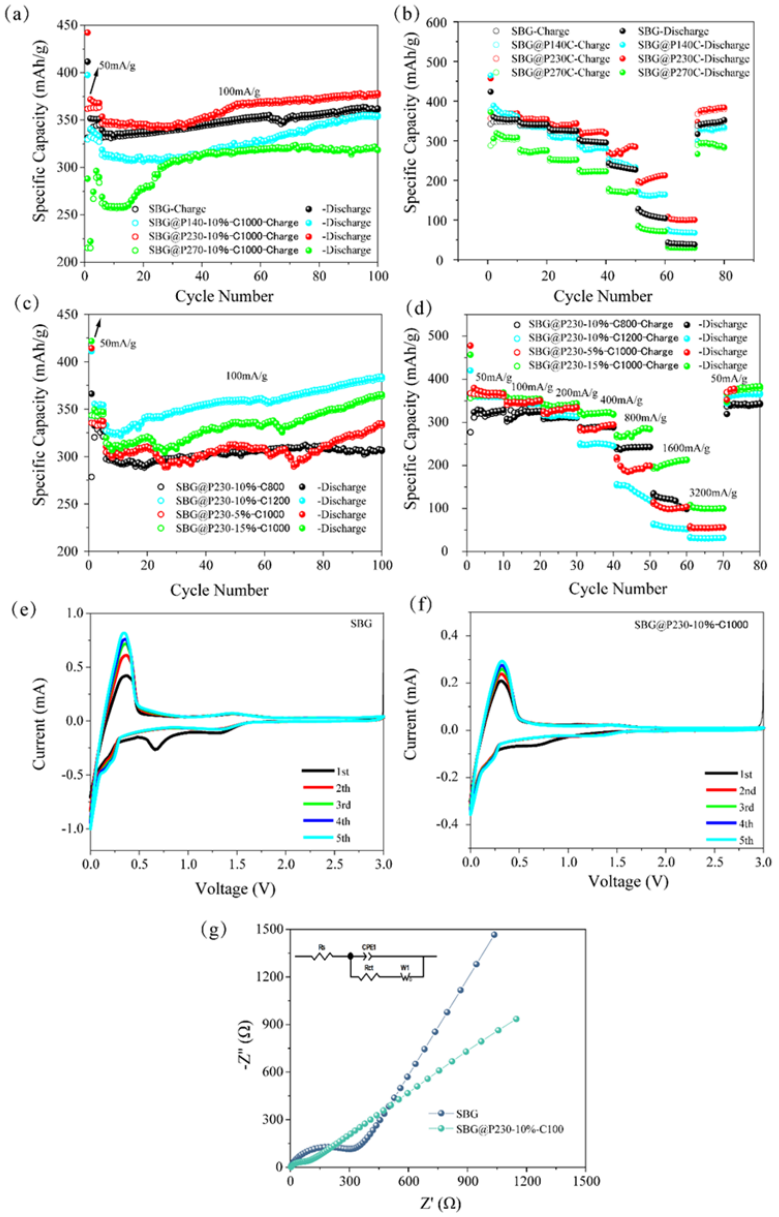

Fig. 4 Cycling performance (a, c) and rate performance (b, d) of SBG and SBG@Px-y%-Cz, CV curves of SBG (e) and SBG@P230-10%-C1000 (f), and Nyquist plots of SBG and SBG@P230-10%-C1000 (g).

Table 3 Comparison of the electrochemical performance of this work with that of recent state-of-the-art graphite anode materials.

Sample	ICE (%)	Rate performance (Capacity (mAh/g) @ current density)	Cycling stability (Capacity retention/reversible capacity, Number of cycles, Current density)
GC-2 [16]	85.00	338.03 (0.5C)	350.2 mAh/g (200,0.5C)
Gr@rGO [37]	80.00	192 (4C)	97% (600,1C)
PO310-2.0–12@NG-10% [38]	91.58	145 (4C)	254 mAh/g (500,0.5C)
DCG-6B [39]	–	112.5 (1000 mA/g)	94.33% (100,100 mA/g)
4MeOBp-Li-prelithiated graphite (4 min) [40]	103.32	293.1 (1000 mA/g)	329.3 mAh/g (150,100 mA/g)
SBG@P230-10%-C1000 (this work)	81.82	104.5 (3200 mA/g)	–
SBG with 20-s Prelithiation (this work)	97.32	–	389.55 mAh/g (100,100 mA/g)

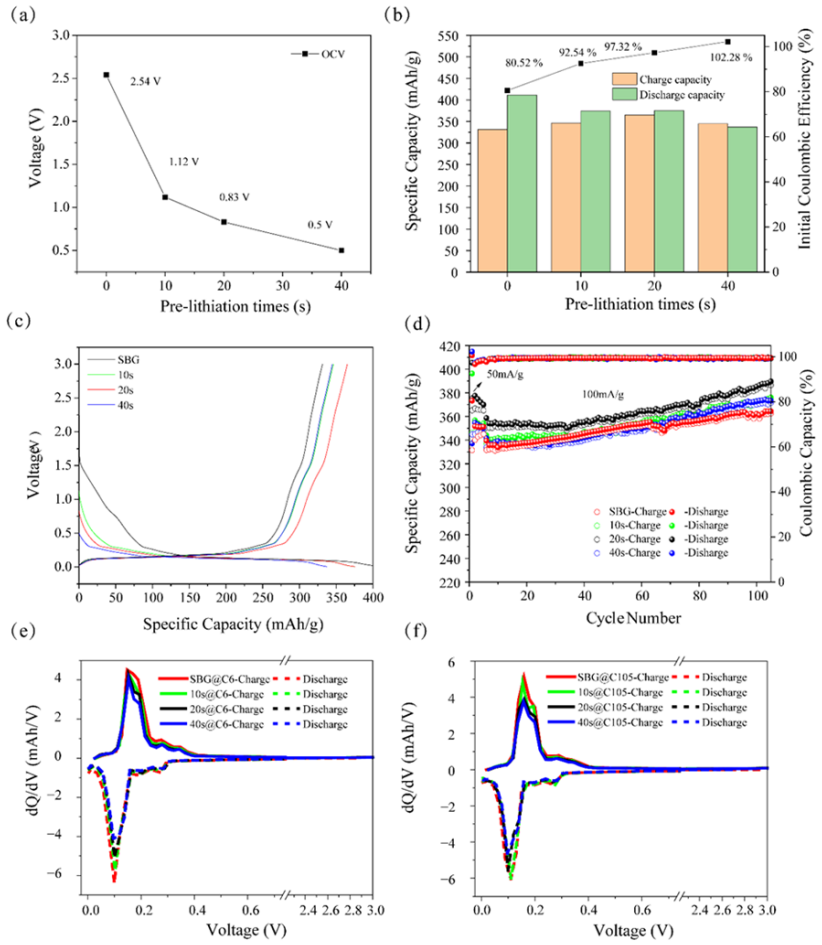

Fig. 5 The electrochemical performances of SBG electrode sheets with different prelithiation times: open-circuit voltage (a); comparison of specific capacity and ICE (b); first constant current discharge-charge curve (c); cycling performances (d); the dQ/dV curves for the sixth cycle charge-discharge curves (e, f).

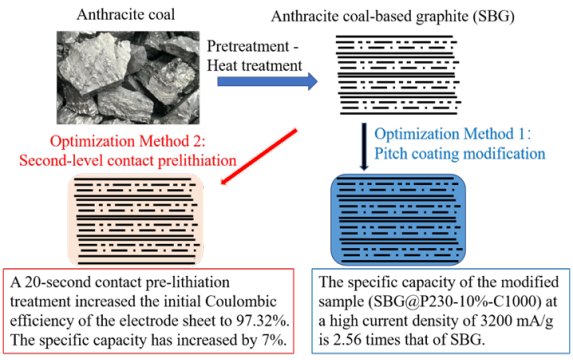

Fig. 6 The modification effects of pitch coating and prelithiation strategies.

comprehensive performance enhancement. The pitch coating (SBG@P230-10%-C1000) halved the specific surface area (from 3.701 to 1.866 m^2/g), which directly reduces the number of active sites for SEI formation. This implies a substantially lower lithium demand for compensation in a subsequent prelithiation step, making the process more efficient and potentially safer, possibly allowing for a shorter prelithiation duration. While the coating alone improved the ICE to 81.82%, an ∼18% irreversible capacity loss remains. It is logically deduced that applying the optimized 20 s prelithiation to the coated material could elevate the ICE close to an ideal 100%, fully addressing the ICE limitation. The sequential strategy of "interface optimization via coating first, followed by precise lithium compensation via prelithiation" thus represents a promising research direction. It is positioned to potentially overcome the dual bottlenecks of coal-based graphite—low ICE and poor rate performance—enabling a substantial leap in anode performance and providing a clear direction for future investigation. The independent optimization of pitch coating and contact prelithiation strategies, as demonstrated above, effectively addresses the specific

limitations of ICE and rate capability in anthracite-based graphite, respectively. To clearly contextualize the performance level achieved in this work, a quantitative comparison of the key electrochemical metrics with representative state-of-the-art graphite anodes reported recently is provided in Table 3.

Compared with state-of-the-art graphite anodes, the independently optimized materials in this work exhibit competitive or even superior performance with notable practical advantages. Contact prelithiation for 20 s boosts ICE to 97.32%, comparable to the most advanced chemical prelithiation (∼103%) but offering distinct merits in processing time (20 s vs. 4 min) and operational simplicity. Separately, the pitch-coated anode (SBG@P230-10%-C1000) delivers an impressive rate capability of 104.5 mAh/g at an ultrahigh current density of 3200 mA/g, on par with graphites modified via complex coating or doping. Critically, these two strategies each present a more energy-efficient and cost-effective route compared to conventional approaches: pitch coating requires only 1000 °C carbonization versus energy-intensive doping processes (e.g., 2800 °C graphitization for B-doping) and contact prelithiation avoids the high complexity and reagent costs associated with chemical prelithiation. This work demonstrates that low-cost anthracite-based graphite can achieve competitive performance through two simple, independently optimized strategies.

CONCLUSION

This study successfully demonstrates the independent efficacy of pitch coating and contact prelithiation for enhancing anthracite-based graphite (SBG) anodes.

The optimized pitch coating constructed a graphitic core-amorphous carbon shell structure, which significantly reduced the specific surface area by 49.6%. This optimization effectively suppressed excessive SEI formation. Coupled with the ion-conductive nature of the amorphous carbon layer, it facilitated rapid ion transport, resulting in a remarkable 2.56-fold increase in rate capability (104.5 mAh/g at 3200 mA/g). In addition, a 20 s contact prelithiation treatment precisely compensated for irreversible lithium loss, elevating ICE from 80.52% to 97.32% and ensuring excellent cycling stability (389.55 mAh/g after 100 cycles). Building upon these individually optimized strategies, their combined application is of significant interest. The coating reduces the active surface area and lithium demand, whereas prelithiation directly addresses irreversible capacity loss. This logical integration highlights a promising path forward to simultaneously address the key limitations of low ICE and poor rate performance in coal-based graphite, meriting further investigation for application in high-performance lithium-ion batteries. It should be noted that the present work was conducted with electrodes of moderate mass loading (∼1.5 mg/cm^2) for fundamental evaluation. Future studies focusing on high-mass-loading electrodes are necessary to address the additional challenges (e.g., charge transport kinetics, mechanical integrity) for practical application, which will be a critical step towards the commercialization of this modified coal-based graphite anode.

Acknowledgements: This work was supported by Fundamental Research Program of Shanxi Province (202403021221003) and Key Research and Development (R&D) Projects of Shanxi Province (202202040201007).

REFERENCES

1. Zhong C, Weng S, Wang Z, Zhan C, Wang X (2023) Kinetic limits and enhancement of graphite anode for fast-charging lithium-ion batteries. *Nano Energy* **117**, 108894.
2. Kongtanawanich K, Likasitwatanakul P, Wattanapanitch M, Jirawatnotai S (2025) Optimization of *in vitro* cell culture conditions suitable for the cholangiocarcinoma stem cell study. *ScienceAsia* **51**, 2025059.
3. Liu H, Duan P, Wu Z, Liu Y, Yan Z, Zhong Y, Wang Y, Wang X (2025) Silicon/graphite/amorphous carbon composites as anode materials for lithium-ion battery with enhanced electrochemical performances. *Mater Res Bull* **181**, 113082.
4. Li L, Qin R, Zhan R, Tu C, Liu X, Liu L, Deng L (2024) Modification with graphite and sulfurized amorphous carbon for high-performance silicon anodes in lithium-ion batteries. *J Energy Storage* **98**, 113196.
5. Liu Y, Shi H, Wu Z (2023) Recent status, key strategies and challenging perspectives of fast-charging graphite anodes for lithium-ion batteries. *Energy Environ Sci* **16**, 4834–4871.
6. Zhao W, Zhao C, Wu H, Li L, Zhang C (2024) Progress, challenge and perspective of graphite-based anode materials for lithium batteries: A review. *J Energy Storage* **81**, 110409.
7. Barre FI, Billy RG, Lopez FA, Müller DB (2024) Limits to graphite supply in a transition to a post-fossil society. *Resour Conserv Recycl* **208**, 107709.
8. Zhao Y, Zhang R, Hao J, Yang X, Chen J, Guo J, Chi C (2025) Understanding the carbonization-controlled microstructure regulation in coal-based hard carbon to strengthen sodium storage performance. *Phy Chem Chem Phys* **27**, 11752–11761.
9. Li Y, Tian X, Song Y, Yang T, Wu S, Liu Z (2022) Preparation and lithium storage of anthracite-based graphite anode materials. *New Carbon Mater* **37**, 1163–1169.
10. Rong T, Yuan Y, Yu H, Zuo H, Xue Q (2023) Research on anthracite-derived graphite flakes prepared by molten salt electrolysis as anode materials for high-performance lithium-ion batteries. *Fuel Process Technol* **252**, 107992.
11. Mukhan O, Yun J-S, Munakata H, Kanamura K, Kim S-S (2024) Quantification of the carbon-coating effect on the interfacial behavior of graphite single particles. *ACS Omega* **9**, 4004–4012.
12. Chen R, Zhang Y, Wang Y, Shen C, Zhan L, Ling L (2024) Modification mechanism of graphite anode in lithium-ion battery coated with ethylene tar pitch. *J Appl Electrochem* **55**, 865–875.

13. Wang Z, Du Z, Wang L, He G, Parkin IP, Zhang Y, Yue Y (2024) Disordered materials for high-performance lithium-ion batteries: a review. *Nano Energy* **121**, 109250.
14. Hou Y, Guo H, Xing B, Zeng H, Kang W, Qu X, Zhang C, Jia J, et al (2024) Purification of spent graphite and surface modification with amorphous carbons as anodes for high-performance lithium-ion batteries. *Fuel* **374**, 132488.
15. Liu P, Peng J, He L, Yang J, Tang Y, Zhou K, Xie Z, Wang X (2024) Amorphous carbon coating enabling waste graphite to reuse as high-performance anode of lithium-ion battery. *ACS Appl Energy Mater* **8**, 442–451.
16. Xiao P, Wang Z, Long K, Yang J, Liu X, Ling C, Chen L, Mei L (2024) Stable cycling and low-temperature operation utilizing amorphous carbon-coated graphite anodes for lithium-ion batteries. *RSC Adv* **14**, 13277–13285.
17. Yu Y, Yang Z, Liu Y, Xie J (2022) Achieving SEI preformed graphite in flow cell to mitigate initial lithium loss. *Carbon* **196**, 589–595.
18. Lin Z, Tong Z, Cai H, Li C, Ding Y, Lv C, Lu M (2025) Prelithiation technology for high energy density lithium-ion batteries: Design, progress, advantages and challenges. *Energy Storage Mater* **83**, 104709.
19. Li S, Jiang J, Feng Q, Zheng Y, Chen Y, Ju Z, Zhuang Q, Wu K, et al Molecular engineering chemical prelithiation reagent with low redox potential for graphite anode enables high coulombic efficiency. *Small* **20**, 2406274.
20. Ünal L, Maccio-Figgemeier V, Haneke L, Eshetu GG, Kasnatscheew J, Winter M, Figgemeier E (2024) Prelithiated carbon nanotube-embedded silicon-based negative electrodes for high-energy density lithium-ion batteries. *Adv Mater Interfaces* **11**, 2400024.
21. Li C, Deng Y, Wang K, Li S, Meng X, Chen M, Liao Y, Xing L, et al (2024) Insight into the enforced stability of the solid electrolyte interphase on the graphite anode by prelithiation. *J Phys Chem Lett* **15**, 9105–9112.
22. Chen S, Wang Z, Zhang M, Shi X, Wang L, An W, Li Z, Pan F, et al (2023) Practical evaluation of prelithiation strategies for next-generation lithium-ion batteries. *Carbon Energy* **5**, e323.
23. Seo SW, Ahn WJ, Kang SC, Im JS (2024) Effect of pitch crystallinity on electrochemical performance of graphite carbon coatings. *J Energy Storage* **81**, 110489.
24. Li K, Liu Q, Cheng H, Hu M, Zhang S (2021) Classification and carbon structural transformation from anthracite to natural coaly graphite by XRD, Raman spectroscopy, and HRTEM. *Spectrochim Acta A Mol Biomol Spectrosc* **249**, 119286.
25. Liu S, Zhang K, Lei L, Yin D, Teng J, Wang Q, Tang X, Gao Y, et al (2025) Two-step optimization of hard carbon anodes via carbonization temperature and chemical vapor deposition for enhanced initial coulombic efficiency and rate performance in Li-ion batteries. *Carbon* **247**, 121022.
26. Wang Y, Li M, Zhao Z, Xu G, Ge Y, Wang S, Bai J (2023) Preliminary exploration of the mechanism governing the cell structure variation of mesophase coal pitch/carbon black composite carbon foam. *Diam Relat Mater* **136**, 110077.
27. Cançado LG, Monken VP, Campos JLE, Santos JCC, Backes C, Chacham H, Neves BRA, Jorio A (2024) Science and metrology of defects in graphene using Raman spectroscopy. *Carbon* **220**, 118801.
28. Guo R, Liu X, Wen B, Liu F, Meng J, Wu P, Wu J, Li Q, et al (2020) Engineering mesoporous structure in amorphous carbon boosts potassium storage with high initial Coulombic efficiency. *Nano-Micro Lett* **12**, 148.
29. Hou L, Xing B, Zeng H, Kang W, Guo H, Cheng S, Huang G, Cao Y, et al (2022) Aluminothermic reduction synthesis of Si/C composite nanosheets from waste vermiculite as high-performance anode materials for lithium-ion batteries. *J Alloy Compd* **922**, 166134.
30. Chen G, Cao D, Liao F, He H, Wang A, Peng S (2025) Preparation and characterization of coal-based graphite from Huyan mountain anthracite by high-temperature simulation. *PLOS One* **20**, e0322558.
31. Srinivasan N R, Al-Rubaye S, Subramaniyam CM (2024) Structural properties and electrochemical performances of mesoporous carbon towards enhanced lithium-ion storage. *Chem Inorg Mater* **2**, 100032.
32. Han Y, Chandio ZA, Soni HL, Ciucci F, Cheong JY (2025) Carbon-derived pitch assisted surface modification of anode materials for lithium-ion batteries: Status and future perspectives. *J Energy Storage* **125**, 116981.
33. Ma C, Hu Z, Song N, Zhao Y, Liu Y, Wang H (2021) Constructing mild expanded graphite microspheres by pressurized oxidation combined microwave treatment for enhanced lithium storage. *Rare Met* **40**, 837–847.
34. Kondo Y,Abe T, Yamada Y (2022) Kinetics of interfacial ion transfer in lithium-ion batteries: Mechanism understanding and improvement strategies. *ACS Appl Mater Interfaces* **14**, 22706–22718.
35. Panchal K, Bhakar K, Sharma KS, Kumar D, Prasad S (2024) Review on electrochemical impedance spectroscopy: A technique applied to hollow structured materials for supercapacitor and sensing applications. *Appl Spectrosc Rev* **60**, 30–55.
36. Dong Y, Wu F, Chen T, Su F, Weng S, Liu C, Yan W, Ma S, et al (2025) Hierarchically conformal Li^+/electron conductive and mechanically robust interface enabling natural graphite anodes for fast-charging and long-cycling operation. *Adv Energy Mater* **15**, 2500978.
37. Xu Q, Guo L, Yu H, Zhang Y, Liu T, Han J, Zhi L (2025) Electronegative interface modification enables accelerated interfacial kinetics for lithium-ion battery anodes. *Carbon* **244**, 120638.
38. Chen R, Zhang Y, Wang Y, Shen C, Zhan L, Ling L (2025) Modification mechanism of graphite anode in lithium-ion battery coated with ethylene tar pitch. *J Appl Electrochem* **55**, 865–875.
39. Chu R, Zhang J, Li S, Tang J, Feng Y, Chen S, Zhu J, Li P, Meng X (2025) Preparation of boron-doped anthracite coal-based graphite for high performance lithium-ion batteries. *Ionics* **31**, 4041–4051.
40. Xu C, Jiang J, Li S, Wang Z, Zhou G, Chen Y, Kong X, Zhuang Q, Ju Z (2025) Molecular tailoring engineering enables stable and efficient chemical pre-lithiation for graphite anodes in lithium-ion batteries. *J Power Sources* **655**, 237971.